Application of Uintah-MPM to shaped charge jet penetration of aluminum

2010 IOP Conf. Ser.: Mater. Sci. Eng. 10 012223

(http://iopscience.iop.org/1757-899X/10/1/012223)

IOP Conf. Series: Materials Science and Engineering **10** (2010) 012223 doi:10.1088/1757-899X/10/1/012223

Application of Uintah-MPM to shaped charge jet penetration of aluminum

J. Burghardt[1], B. Leavy[1], J. Guilkey[2], Z. Xue[2], R. Brannon[1]

[1] University of Utah, 50 S. Central Campus Dr. Room 2110, Salt Lake City, UT 84112
[2] Schlumberger Technology Corporation, 14910 Airline Road, Rosharon, TX 77583

E-mail: j.burghardt@utah.edu

Abstract. The capability of the generalized interpolation material point (GIMP) method in simulation of penetration events is investigated. A series of experiments was performed wherein a shaped charge jet penetrates into a stack of aluminum plates. Electronic switches were used to measure the penetration time history. Flash x-ray techniques were used to measure the density, length, radius and velocity of the shaped charge jet. Simulations of the penetration event were performed using the Uintah MPM/GIMP code with several different models of the shaped charge jet being used. The predicted penetration time history for each jet model is compared with the experimentally observed penetration history. It was found that the characteristics of the predicted penetration were dependent on the way that the jet data are translated to a discrete description. The discrete jet descriptions were modified such that the predicted penetration histories fell very close to the range of the experimental data. In comparing the various discrete jet descriptions it was found that the cumulative kinetic energy flux curve represents an important way of characterizing the penetration characteristics of the jet. The GIMP method was found to be well suited for simulation of high rate penetration events.

1. Introduction

Numerically solving the equations of motion during a penetration event presents many unique challenges. Penetration by definition involves massive deformations, which leads to mesh distortion and entanglement problems with standard Lagrangian finite-element algorithms. The conventional alternative to a Lagrangian scheme is to adopt an Eularian approach to solving the equations of motion. However, under the large deformations experienced in a penetration event most materials of interest will undergo significant plastic deformation, which typically adds a history dependence to material response. This history dependence is often expressed using internal state variables such as plastic strain, damage, etc. These internal state variables are necessarily properties of each Lagrangian material element. Advection schemes used in a conventional Eularian approach cause the field of internal state variables to become corrupted and results in nonphysical responses such as numerical healing. The material point method (MPM) [1] was proposed as a method which retains the advantages of both Eularian and Lagrangian techniques. The MPM subdivides the problem domain into a set of Lagrangian material point particles. All state data is stored on the material point particles, but the equations of motion are solved on a fixed Eularian grid. A set of interpolation functions is used to transfer information between the Lagrangian particles and the Eularian grid. As originally proposed the MPM suffered from a cell crossing instability for large displacement problems which is caused

by a discontinuity in the gradient of the interpolation functions. The generalized interpolation material point (GIMP) method [2] uses a smoother interpolating function which drastically reduces the cell crossing instability. The GIMP method has successfully been used in a wide range of large deformation applications [3–11]. Recently, an alternative or generalization of the GIMP method has been developed to account for deformation of particle domains [12], although this extension was not used in the current work. This paper describes an application of the GIMP method to the simulation of shaped charge jet penetration into aluminum. Experimental data for the jet properties are used to develop two discrete models of the jet. Comparison of the results of simulations using both of these jet descriptions are used to determine what effect various jet characteristics have on the penetration behavior of the shaped charge jet. The penetration time history from these simulations are also compared with experimentally measured penetration time histories.

2. Methods

2.1. Jet properties

The properties of the shaped charge jet in free flight were measured using an x-ray technique. The details of this measurement are not discussed here, but the results of these measurements are used to develop several discrete representations of the shaped charge jet in flight. Figure 1 contains a plot of the experimentally measured normalized jet radius $\bar{r}$ along the length of the jet. The normalized jet radius is given by

$$\bar{r} = \frac{r}{r_{\max}} \tag{1}$$

where r is the actual radius, and $r_{\max}$ is the maximum measured radius (whose value is not given here for proprietary reasons). The normalized distance along the jet $\bar{x}$ is given by

$$\bar{x} = \frac{x}{L_{\text{jet}}} \tag{2}$$

where x is the actual distance along the jet and L_{jet} is the length of the jet at the instant of measurement. Normalized time $\bar{t}$ is also defined as

$$\bar{t} = \frac{t}{t_{\max}} \tag{3}$$

where $t_{\max}$ is the time at which penetration is complete and t represents the actual time. The radius data were fit using both a bi-linear and a simple linear approximation to the radius as shown in Figure 1a. The average mass density of the jet along its length was also measured. The experimentally measured normalized jet density data and the two approximating curves are shown in Figure 1b. Similar to the normalized radius, the normalized jet density $\bar{\rho}$ is given by

$$\bar{\rho} = \frac{\rho}{\rho_{\max}} \tag{4}$$

where ρ is the actual density and $\rho_{\max}$ is the maximum measured density. For the density a bi-linear fit was used as well as a constant density fit. The use of these curves will be discussed in section 2.2.

2.1.1. Interpretation of jet data A shaped charge jet in free flight is very complex and dynamic. While the measurement of the radius, density and velocity along the length of the jet in free flight is a significant accomplishment, it represents an incomplete description of the jet properties. For example, the density and velocity of the jet material undoubtedly vary across the cross-section of the jet. However, the experimental data represent an average density and velocity across the

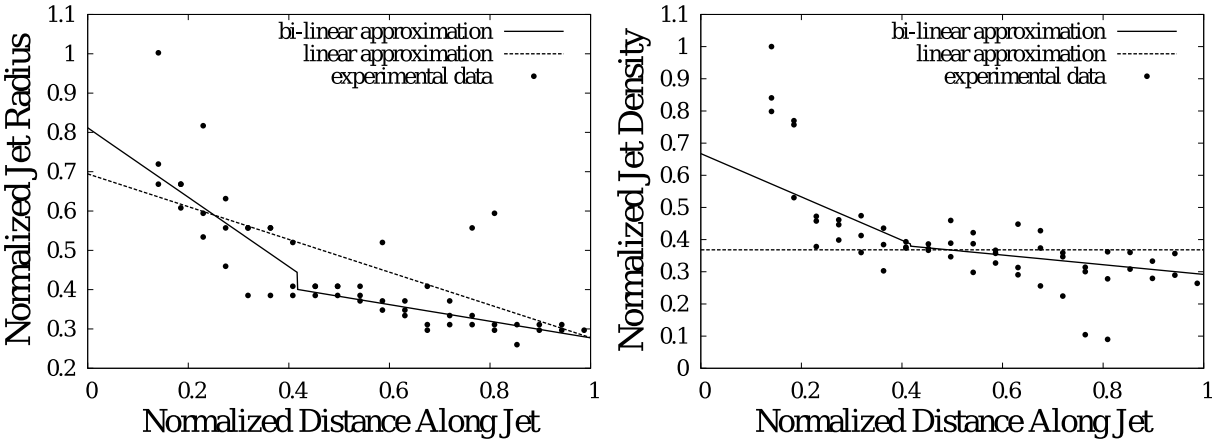

Figure 1. Experimentally measured normalized jet radius $\bar{r}$ and density $\bar{\rho}$ vs. normalized distance along the length of the jet $\bar{x}$. The solid line is a bi-linear approximation to the radius and density data and the dashed line is a linear approximation to the radius data and a constant valued approximation to the density data.

cross-section of the jet. Therefore, certain approximations and assumptions are necessary to develop a more complete model of the jet behavior. Consistent with trends evident in the data and/or consistent with sensitivity studies of simulation results, the assumptions made in this study are:

(i) the velocity of the jet is unidirectional
(ii) the velocity of each material particle in the jet is constant throughout the evolution of the jet (i.e., the particles are in free flight with negligible aerodynamic drag)
(iii) the velocity varies linearly from the tip to the tail of the jet
(iv) the velocity and density are uniform across the width of the jet
(v) the strength of the jet material is inconsequential to the penetration behavior of the jet

The first three assumptions are justified by behavior evident in the x-ray measurements, where, for example, it is seen that radial motion is negligible. The fourth assumption is a simplification which is made largely due to a lack of data regarding the distribution of the density and velocity across the cross-section of the jet. Validating the fifth assumption is one of the major contributions of this study. It is postulated that quantities such as the cumulative momentum and/or kinetic energy flux are more critical than jet strength in determining the penetration behavior of the jet. This postulate will be discussed further below.

With these assumptions, the length, radius, density and velocity distributions within the jet may be computed for any time based on the experimental data. As mentioned above, the experimental data were taken for a jet in free flight where the length of the jet when measured is much greater than the standoff distance which is typically used with shaped charge jets. The standoff distance is defined to be the distance between the face of the shaped charge and the target at the time of detonation. Since the x-ray measurements are made at a larger standoff than is used in the penetration tests, the experimental jet data are extrapolated backward in time to model the standoff distances actually used in the penetration tests. This is done by recognizing that, with a constant particle velocity, the axial component of the deformation gradient is given by:

$$F = 1 + V_{\text{tip}} \frac{t}{L_{\text{o}}} \tag{5}$$

where V_{tip} is the velocity at the tip of the jet, t is time, and L_o is the length of the jet in the reference configuration. For convenience the reference configuration will be taken to be the configuration where jet properties were measured. The deformation gradient may then be used to transform the expressions that were fit to the experimental data backward in time to represent a shorter standoff distance. These extrapolated jet data are used to inform the development of the discrete jet descriptions. Hereafter, all references to the projected jet refer to the bi-linear fit to experimental data projected backward in time to the standoff distance used in the experimental penetration tests.

2.2. Discrete Jet Descriptions

The actual shaped charge jet considered in this study is a powdered metal jet composed of three different materials. The size of the metal particles that compose the jet is such that they are too small to be individually resolved in the discrete simulation. As such, several schemes were developed to describe the jet material using the GIMP method. Based on the postulate that the cumulative momentum and/or kinetic energy flux provided by the jet are more important to the penetration behavior than the strength of the jet, the discrete jet descriptions used in this study are very simplistic. The two methods used are described below.

2.2.1. Single Stream of Cylinders One approach that was used to construct a discrete description of the jet was to use a single stream of cylinders with varying radius and velocity. The radius of each cylinder in the jet was prescribed according to the bi-linear approximation shown in Figure 1a. The density of each cylinder was prescribed to be the density of the solid metal from which the majority of the jet is composed. To account for the reduced density of the particulated metal jet, void space was added between the cylinders as shown in Figure 2. The length of each cylinder was chosen such that the effective density over each jet segment would correspond to the projected jet density for that location in the jet. The effective density is defined as

$$\rho_{\text{eff}} = \frac{V_{\text{cyl}}\, \rho_{\text{H}}}{V_{\text{cyl}} + V_{\text{void}}} \tag{6}$$

where V_{cyl} is the volume of a given cylinder, V_{void} is the void space surrounding that cylinder, and ρ_H is the density of the cylinder material. The length of each segment in the jet (and consequently the number of cylinders in the jet) is then a free parameter which was found to be significant as discussed below. As the strength of the jet material is assumed to be inconsequential, all constitutive parameters for the cylinders except density were set to be those of the solid metal of which the majority of the jet is composed. This assumption was tested by drastically changing the yield strength of the jet material in the two simulations discussed below.

As the kinetic energy, momentum and mass flux into the target are thought to be the critical jet characteristics, the cumulative mass, momentum and kinetic energy fluxes as a function of time for the projected jet and each of the discrete jet descriptions were compared. Figure 3 shows plots of the cumulative mass, momentum and kinetic energy fluxes for the projected jet and the two discrete jet descriptions.

2.2.2. Single Stream of Spheres Another method used to simulate the jet in the GIMP model is to simply create a single stream of spheres of varying radius, velocity and density. The radius of the spheres varies according to the linear approximation to the experimentally measured radius data. The velocity of each sphere was prescribed using a linear approximation to experimental

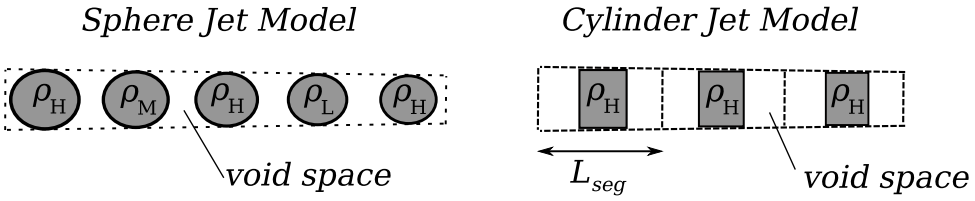

Figure 2. Schematic of the two different discrete jet descriptions used in the simulations where ρ_H, ρ_M and ρ_L correspond to the densities of the three materials which compose the jet. L_{seg} is the length of each segment of the cylinder jet description.

velocity data, however it was fit to the upper end of the experimental data. For this reason the velocity near the tail of the sphere jet is higher than that used in the cylinder jet description. This can be seen as an increase in the momentum and kinetic energy flux relative to the cylinder jet values as seen in Figure 3. Since the actual jet is composed of several distinct material types of various densities, the spheres in this discrete model were also modeled as three distinct materials. Every group of five spheres in the jet was composed of three high density spheres, one medium density sphere, and one low density sphere as shown in Figure 2. The density of this collection of spheres plus the void space around the spheres resulted in th constant mean density shown in Figure 1b. Since the spheres do not allow the radius and length of the jet to be independently controlled, this jet description is not capable of being scaled to an earlier standoff distance since as the jet was shortened the spheres would either overlap or their radius would need to be reduced. For this reason the sphere jet description represents the full length of the measured jet in free flight. While this jet description clearly does not reflect an accurate description of the actual short standoff jet in the penetration tests, comparison of the results of simulations using this jet description with the cylinder jet description does provide some interesting results.

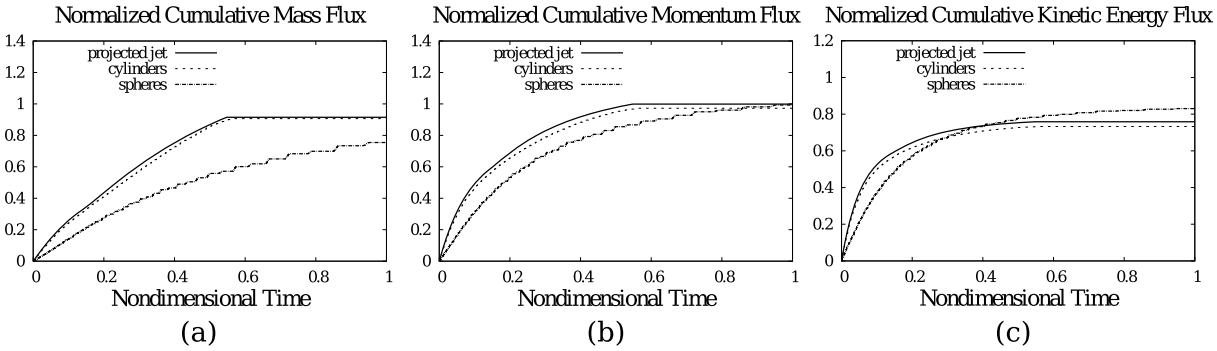

Figure 3. Plot of cumulative mass (a), momentum (b), and kinetic energy (c) flux into the target as a function of time for the projected jet and the two discrete models.

2.3. Target Description

A Johnson-Cook plasticity/damage model [13], as well as an MTS model [14] were used to model the behavior of the aluminum target. The results using both models were nearly indistinguishable. In order to speed up the calculation, four particles per cell (two in the axial direction, two in the radial direction) were used near the penetration channel and a single particle per cell was used far away from the penetration channel.

2.4. Measurement of Penetration Time History

As a validation test laboratory measurements of the penetration time history were made. A stack of aluminum plates was used, some of which were separated by a thin electronic switch as shown in Figure 4. The electronic switch is designed such that when it is perforated it completes a circuit. The time at which each circuit is completed is then recorded, creating a penetration time history. Several tests were performed using 20 switches, 16 switches, 14 switches, and zero switches. In general as more switches were used, the final penetration depth decreased. The test with no switches resulted in a approximately a 15% greater final penetration depth than the average of all of the tests with switches. In contrast the maximum spread in final penetration depth between all of the tests with the various numbers of switches was less than 5% of the average value. In one case a test with 20 switches resulted in a slightly greater penetration depth than an otherwise identical test with 14 switches. In all other cases, tests with more switches yielded less penetration depth than tests with fewer switches. Two different (but relatively short) standoff distances were also used in the tests. Although the standoff distances used in these tests made a relatively small difference in the final depth of penetration, generally the shorter standoff distance resulted in a larger depth of penetration.

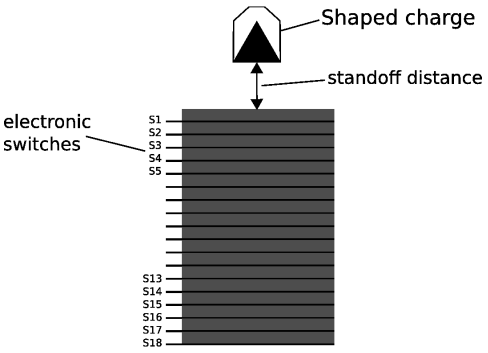

Figure 4. Sketch of the experimental apparatus used to measure the penetration time history. The shaped charge was placed on top of a stack of aluminum plates. An electronic switch was placed between some of the plates. Each switch completes a circuit when it is perforated, thus providing a means of determining when the penetrator reaches each location within the target.

3. Results

The shaped charge jet simulations were performed with both an axisymmetric 2D formulation and a full 3D formulation using the Uintah MPM code with the GIMP interpolator. Figure 5 shows the penetration time history for the axisymmetric cylinder and sphere jet descriptions along with the range of experimental data. A mesh resolution of 0.25 mm in all directions was used in these simulations. Convergence studies are underway, but currently numerical difficulties are plaguing the highest resolution simulations. These difficulties may be resolved by using the method proposed in [12]. As can be seen in Figure 5, the cylinder jet description under-predicts the penetration depth from $\bar{t} \approx 0.25$ through $\bar{t} \approx 0.65$. The sphere jet description predicts the penetration time history more accurately than the cylinder description until $\bar{t} = 0.6$, where it begins to over-predict the penetration depth. This is likely due to the extra momentum flux that this jet description provides at late times as shown in Figure 3b.

As mentioned above, the length of each segment of the cylinder jet, and consequently the number and length of the cylinders was found to be an important parameter. If the segment length was chosen such that the length of each cylinder was approximately the same as its radius, the penetration depth was drastically under-predicted. As the length of each segment and consequently the length of each cylinder was decreased so that the cylinders became thin disks, the depth of penetration curve converged to the one shown in Figure 5. Many thin disks would better approximate, albeit crudely, the actual behavior of a powdered metal jet in that it would provide a series of many smaller impulses rather than fewer large impulses.

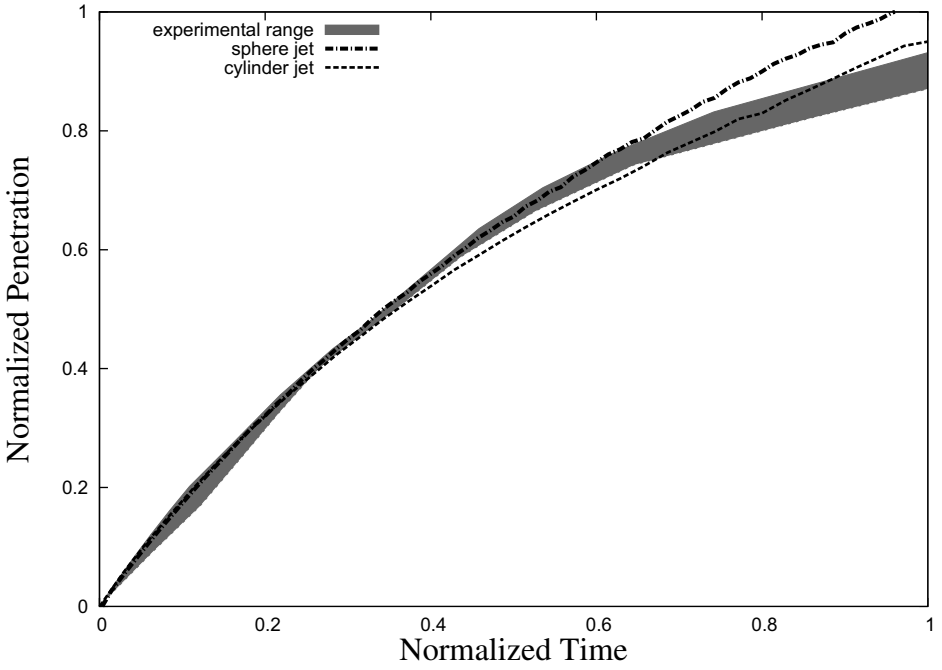

Figure 5. Penetration time history from the experimental data and simulations using the two discrete jet descriptions

As mentioned above, the elastic properties and yield strength of the jet material were assumed to be of little importance. To test this, the simulation using the cylinder jet description was repeated with the yield strength of the jet material cut in half. The resulting penetration time history curve was almost indistinguishable from the original simulation with the full strength jet material. This seems to validate the assumption that the mechanical behavior of the jet material is unimportant, and that the mass, momentum and/or kinetic energy flux that it provides is much more important.

Comparing the cumulative mass and momentum flux curves in Figure 3a and 3b, it can be seen that the sphere jet curves fall below both the cylinder jet and projected jet data curves. Comparing the mass and momentum flux curves to the penetration time history curves in Figure 5 it can be seen that the cylinder jet, sphere jet, and experimental data agree quite well until approximately $\bar{t} \approx 0.25$ at which point the sphere jet begins to penetrate at a greater rate than the cylinder jet curve. This trend continues for the rest of the simulation with the sphere jet predicting a greater final depth of penetration than either the experimental data or the cylinder jet simulation. Since both the cumulative mass and momentum flux curves for the sphere jet fall below those of the cylinder and projected jet curves, this seems to indicate that the mass and momentum flux curves are not good indicators of the penetration behavior of a projectile. In contrast it is observed that the cumulative kinetic energy curves follow a trend that is similar to the penetration curves. That is, the cumulative kinetic energy curve for the sphere jet simulation climbs above both the cylinder jet and projected jet curves at approximately $\bar{t} \approx 0.4$. The sphere jet penetration curve in Figure 5 climbs above the range of experimental data at approximately $\bar{t} \approx 0.6$. This seems to suggest that the cumulative kinetic energy flux is a better predictor of penetration behavior than is the cumulative mass and momentum flux.

Due to the high computational cost only one simulation was performed using a full 3D formulation. This simulation used the sphere jet model and the penetration history curves agreed with the results of the 2D axisymmetric formulation to within 1%. Figure 6 is a collection of

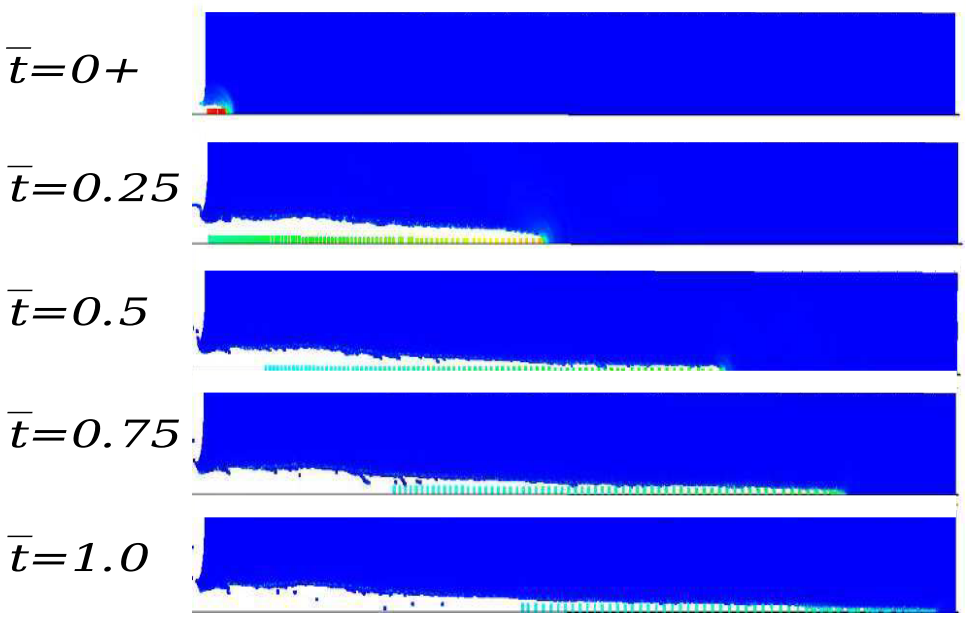

Figure 6. Images of the axisymmetric simulation using the cylinder jet model at various instants in time. The plots are colored according to the magnitude of the velocity vector. The first image labeled $\bar{t} = 0+$ is a very short time after the penetration has begun.

images throughout the 2D axisymmetric simulation using the cylinder jet model. It is apparent in the last image in the figure that not all of the jet has impacted the target. However, the remaining jet material does not increase the depth of penetration when it impacts the target.

4. Conclusion

Tests were performed to measure the radius, density and velocity along the length of a shaped charge jet in free flight. The jet data were projected backward in time under the assumption that the velocity distribution is unidirectional and varies linearly from the tip to the tail of the jet, and that the velocity of each material particle is constant throughout the jet evolution. By projecting the velocity, radius and density data backward in time the effective jet properties are calculated for any standoff distance. The same type of shaped charge jet was used to penetrate into a stack of aluminum plates which were fitted with electronic switches. These switches were used to measure the penetration time history for the shaped charge jet.

The experimental data for the jet properties were used to develop two different discrete models of the jet using the GIMP method. One of these discrete jet descriptions used a single stream of cylinders and the other used a single stream of spheres with the density and velocity of each projectile being set according to the experimental jet data. These models were developed under the assumption that the elastic properties and yield strength of the jet material are not important to the penetration behavior of the jet. This assumption was tested by repeating a penetration simulation with the yield strength of the jet material reduced by 50%. It was found that the penetration time history curve was indistinguishable (i.e., less than 1% difference) from the original simulation with a full strength jet. The jet characteristic which appears to be the best indicator of penetration behavior is the cumulative kinetic energy flux curve. This curve correlated best with the penetration time history curves of the two jet descriptions. It was also found that the axial length of the cylinders in the cylinder jet model (and consequently

the number of cylinder) was an important parameter. Many thin cylinders duplicated the experimentally observed penetration time history better than fewer thick cylinders. This is thought to be due to the fact that many thin cylinders will provide many smaller impulses rather than fewer large impulses, and would thereby better replicate the behavior of a particulated metal jet.

The penetration simulations using the cylinder jet description were able to accurately reproduce the measured penetration time history for the first third of the history. For intermediate times these simulations under-predicted the penetration depth, and at late times the penetration depth is slightly over-predicted. The sphere jet description accurately predicts the penetration time history for the first three-quarters of the history, then over-predicts the final depth of penetration. This is thought to be due to the slightly higher velocity used in the tail section of the sphere jet which causes more kinetic energy to be deposited into the target at late times than the jet measurements indicate. Since the simulation does not include the switches used in the penetration experiments, a greater penetration depth is to be expected.

The GIMP method was found to be well suited to simulation of high-rate penetration events, and this simulation method is likely to be further improved with recent advances that account for massive particle deformations [12]. Considering the degree of uncertainty in the jet characteristics, an appropriate avenue for future work would be to describe the range of results associated with the uncertainty of the inputs.

References

[1] Sulsky D 1994 *Computer Methods in Applied Mechanics and Engineering* **118** 179

[2] Bardenhagen S and Kober E 2004 *Comput. Model. Eng. Sci.* **5** 477–495

[3] York A, Sulsky D and Schreyer H 2000 *International Journal for Numerical Methods in Engineering* **48** 901–924

[4] Love E and Sulsky D 2005 *International Journal for Numerical Methods in Engineering* **65** 1608–1638

[5] Nairn J 2003 *Computer Modeling in Engineering and Sciences* **4** 649–663

[6] Guo Y and Nairn J 2006 *Computer Modeling in Engineering and Sciences* **16** 141–155

[7] Sulsky D, Schreyer H, Peterson K, Kwok R and Coon M 2007 *Journal of Geophysical Research* **112** CiteID C02S90

[8] Ma S, Zhang X and Qiu X 2009 *International Journal of Impact Engineering* **36** 272–282

[9] Zhang H, Wang K and Chen Z 2009 *Computer Methods in Applied Mechanics and Engineering* **198** 1456–1472

[10] Schreyer H, Sulsky D and Zhou S 2002 *Computer Methods in Applied Mechanics and Engineering* **191** 2483–2507

[11] Daphalapurkar N, Lu H, Coker D and Komanduri R 2007 *International Journal of Fracture* **143** 79–102

[12] Sadeghirad A, Brannon R and Burghardt J 2010 *International Journal for Numerical Methods in Engineering* (Under Review)

[13] Johnson G and Cook W 1985 *Engineering Fracture Mechanics* **21** 31 – 48 ISSN 0013-7944 URL `http://dx.doi.org/10.1016/0013-7944(85)90052-9`

[14] Follansbee P and Kocks U 1988 *Acta Metallurgica* **36** 81 – 93 ISSN 0001-6160 URL `http://dx.doi.org/10.1016/0001-6160(88)90030-2`